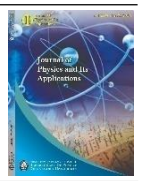
Journal of Physics and Its Applications

Journal homepage : https://ejournal2.undip.ac.id/index.php/jpa/index



Surface-Enhanced Raman Spectroscopy with $La_{0.5}Bi_{0.5}FeO_3$-Based Substrates for Paraquat Pesticide Detection

Nia Tiawati[1, 2], Djoko Triyono[1*], and Muhandis Shiddiq[2]

[1]*Department of Physics, Faculty of Mathematics and Natural Sciences, Universitas Indonesia, Depok, Indonesia.*
[2]*Research Center for Photonics, National Research and Innovation Agency (BRIN), Tangerang Selatan, Indonesia.*

[*]*Corresponding author: djoko.triyono@sci.ui.ac.id*

ARTICLE INFO

Article history:
Received: 14 March 2025
Accepted: 21 May 2025
Available online: 31 May 2025

Keywords:
SERS
$La_{0.5}Bi_{0.5}FeO_3$
Perovskite
Substrate
Paraquat

ABSTRACT

Paraquat is a highly toxic herbicide that poses serious environmental and health risks. Conventional detection methods are accurate but often complex and time-consuming. This study explores the use of $La_{0.5}Bi_{0.5}FeO_3$ (LBFO) perovskite as a novel Surface-Enhanced Raman Spectroscopy (SERS) substrate. LBFO was synthesized via a sol-gel method and characterized using XRD, XRF, UV-Vis, and Raman spectroscopy. The LBFO-based substrate successfully enhanced the Raman signals of paraquat, enabling detection at concentrations as low as 6 ppm. These results suggest the feasibility of LBFO as an effective and low-cost SERS substrate for rapid paraquat detection.

1. Introduction

Paraquat is a potent herbicide widely used for effective weed control, helping to reduce labor and increase agricultural yields globally [1]. However, it is highly toxic to humans, causing damage to vital organs such as the lungs, liver, heart, and brain [2]. Additionally, its persistent residues in agriculture pose a global health threat [3]. Rapid, reliable, and accurate detection is crucial to ensure human health safety, making the monitoring of paraquat levels extremely important. Conventional detection methods for paraquat residues include the use of Gas Chromatography-Mass Spectrometry (GC-MS) [4], High-Performance Liquid Chromatography (HPLC) [5], and Liquid Chromatography-Tandem Mass Spectrometry (LC-MS/MS) [6]. These methods typically offer the required accuracy and precision; however, they also have several drawbacks, such as being time-consuming, complex in operation, and expensive [3].

Surface-Enhanced Raman Spectroscopy (SERS) is a highly sensitive analytical technique that significantly amplifies Raman scattering signals when light interacts with metal nanoparticle surfaces, typically noble metals such as gold (Au) or silver (Ag). This enhancement is primarily attributed to surface plasmon resonance (SPR), where collective oscillations of conduction electrons intensify the local electromagnetic field around the nanoparticles [7]. Despite its sensitivity, detecting pesticides using SERS remains challenging due to the weak affinity between pesticide molecules and metal surfaces. Many pesticides exhibit low polarity and possess few functional groups capable of forming strong interactions with metals, resulting in diminished signal intensity and reduced detection sensitivity. Furthermore, the use of noble metals like gold and silver adds to the overall cost, limiting the practicality of SERS for large-scale or routine applications [3].

To overcome this limitation, the development of cost-effective SERS substrates with strong adsorption capabilities, such as perovskite-based materials, has gained increasing attention for the effective detection of pesticide residues. The enhancement of Raman signals in perovskite-based SERS systems is primarily attributed to photoinduced charge transfer mechanisms. Additionally, the perovskite film acts as an intermediate layer that mitigates the rapid attenuation of electromagnetic fields, thereby contributing to signal amplification [8].

However, many types of perovskites contain lead (Pb), which is highly toxic. Therefore, it is important to study lead-free perovskites as potential substrates for SERS. In this study, we synthesized and characterized a lead-free perovskite, $La_{0.5}Bi_{0.5}FeO_3$ (LBFO), to investigate its ability as a SERS substrate to detect paraquat. To the best of our knowledge, there have been no prior reports on the synthesis and performance of the $La_{0.5}Bi_{0.5}FeO_3$ as a SERS substrate for paraquat detection.

2. Methods

2.1. Synthesis of $La_{0.5}Bi_{0.5}FeO_3$

$La_{0.5}Bi_{0.5}FeO_3$ nanoparticles were synthesized using the sol-gel method with citric acid, as described by Triyono and his team [cite]. The raw

materials, (what is the raw materials?), were dissolved in monohydrate citric acid at 120 °C for 24 hours using a magnetic stirrer. The solution was then dried and heated at 175 °C for 12 hours to obtain nanoparticle powder. Finally, the nanoparticles were calcined at 900 °C for 6 hours to enhance crystallization and uniformity [9].

2.2. Fabrication of $La_{0.5}Bi_{0.5}FeO_3$

Silicon substrates (1 cm × 1 cm) were cleaned using an ultrasonic cleaner (40 kHz) with ethanol, isopropanol, and aquabidest for 15 minutes with each solvent. A total of 200 mg of $La_{0.5}Bi_{0.5}FeO_3$ nanopowders were dissolved in 5 mL of solvent, consisting of 3.5 mL isopropanol and 1.5 mL of aquabidest. The solution was stirred and heated at 100°C for 2 hours. The synthesized $La_{0.5}Bi_{0.5}FeO_3$ sample was used as the material for the SERS substrate. The process began by taking 500 µL of the $La_{0.5}Bi_{0.5}FeO_3$ solution to be deposited onto the silicon substrate. The solution was then dropped and spread over the Si substrate using the drop-casting method, followed by drying at 100 °C. The SERS sample was prepared by depositing a paraquat molecule solution onto the prepared $La_{0.5}Bi_{0.5}FeO_3$ substrate.

2.3. Characterization of $La_{0.5}Bi_{0.5}FeO_3$

For the crystal structure analysis of $La_{0.5}Bi_{0.5}FeO_3$ samples, X-Ray Diffraction (XRD) measurements were performed using a PANalytical X'Pert Pro with a Cu Kα radiation source (λ = 1.5418 Å) and Bragg angles ranging from 15° to 90°. Elemental analysis was conducted using a PANalytical ε1 X-Ray Fluorescence (XRF) instrument, equipped with an Ag radiation source and operating at 50 kV. Optical properties were measured using an Agilent Technologies Cary 100 UV-Visible spectrophotometer. Raman spectroscopy was performed using a HR550 Horiba Jobin Yvon system with 785 nm laser excitation.

3. Results and Discussion

3.1. X-Ray Diffraction (XRD) Analysis

The XRD pattern of $La_{0.5}Bi_{0.5}FeO_3$ was analyzed using Highscore Plus software, and the results were found to be in excellent agreement with the standard reference (ICSD 98-016-0736) [10]. The XRD pattern for $La_{0.5}Bi_{0.5}FeO_3$ nanoparticles is shown in Fig. 1. The figure displays the XRD pattern with distinct peaks, free from impurities, indicating that Bi^{3+} has successfully substituted $LaFeO_3$ in the perovskite lattice. The analysis indicates that the material has an orthorhombic structure and a *Pnma* space group, with no additional phases or impurities detected. Details of the crystal structure can be found in Table 1.

The Rietveld refinement curve of the XRD pattern of $La_{0.5}Bi_{0.5}FeO_3$ demonstrates good agreement between the experimental data and the calculated values, with minimal differences, which are clearly visible on the green difference curve. The calculated goodness-of-fit value (χ^2) is 1.4, which is close to unity, indicating a strong correlation between the measured and simulated XRD patterns [12].

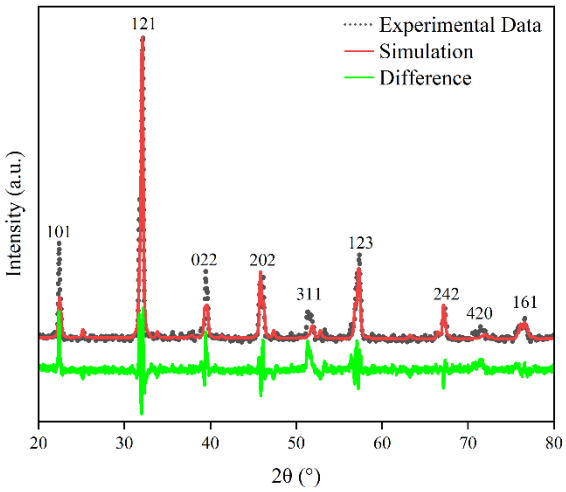


Fig. 1: XRD patterns of $La_{0.5}Bi_{0.5}FeO_3$ nanoparticles

To determine the extent of distortion or shape change in the sample, the tolerance factor and tilt angle are calculated based on the bond length and angle data presented in Table 1. The obtained tolerance factor indicates a slight distortion of the crystal structure. Additionally, the decrease in the tilt angle indicates an increase in the force that drives the octahedral tilting [13].

Table 1: The crystalline structure parameters of $La_{0.5}Bi_{0.5}FeO_3$ nanoparticles

Parameter	Value
Crystallographic Parameters	
Lattice Parameters	
a (Å)	5.617
b (Å)	7.846
c (Å)	5.5615
χ^2	1.4338
Crystallite size (nm)	38.34
Density (g/cm^3)	6.5776
Volume (V/10^6 pm^3)	245.097
R factor (%)	
Re	5.344
Rp	5.452
Rwp	7.663
Geometrical parameters	
Bond Length (Å)	
La/Bi-O1	2.5695
La/B-O2	2.4044
<La/Bi-O>	2.487
Fe-O1	1.9795
Fe-O2	2
<Fe-O>	1.9898
Bond Angle (°)	
La/Bi-O1-La/Bi	167.6311
La/Bi-O2-La/Bi	103.0734
Fe-O1-Fe	162.104
Fe-O2-Fe	157.4670
Tolerance Factor	0.8838

Based on the results from the Highscore Plus software, the data obtained is presented in the form of CIF files using VESTA. VESTA is employed to assist in visualizing the crystal structure [14]. Fig. 2

illustrates the geometric parameters of the crystal structure of the sample, which were obtained using VESTA software from the raw data. From the figure, it can be observed that sample exhibit a distorted orthorhombic crystal structure. The $La_{0.5}Bi_{0.5}FeO_3$ structure adopts the ABO_3 perovskite structure, where La/Bi cations are located at the A-site in a cubic-octahedral arrangement, while Fe occupies the B-site and is coordinated with six oxygen ions to form an octahedral structure.

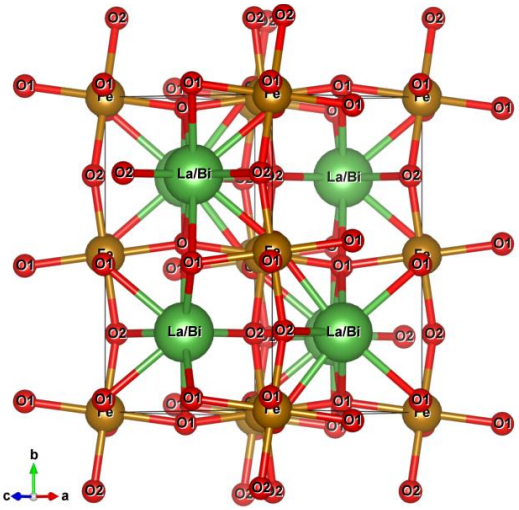


Fig. 2: The crystalline structure of the perovskite orthorhombic material $La_{0.5}Bi_{0.5}FeO_3$ powder sample

3.2. X-Ray Fluorescence (XRF)

To determine the atomic composition, the sample was examined using X-Ray Fluorescence (XRF) analysis. Table 2 presents the composition of the $La_{0.5}Bi_{0.5}FeO_3$ sample after calcination at 900 °C. Hydrogen through fluorine were not detected by XRF, and therefore, the oxygen atomic calculation is not included in the table. This limitation arises from the nature of XRF, as it is more effective in detecting elements with higher atomic numbers. The results indicate that the weight percentage obtained from the experiment are similar to the stoichiometry calculated weight percentage. Table 2 also compares the atomic ratio percentages obtained from the experiment with the calculated values. The results show that the experimental atomic ratio percentage is slightly higher than the calculated value, although the difference is not significant.

Table 2: XRF characterization for $La_{0.5}Bi_{0.5}FeO_3$ nanoparticles

%Weight					
XRF Measurements			**Stoichiometric Calculation**		
La	Bi	Fe	La	Bi	Fe
29.31	48.50	22.19	30.22	45.47	24.31
Atomic Ratio					
XRF Measurements			**Stoichiometric Calculation**		
La	Bi	Fe	La	Bi	Fe
0.5	0.55	0.95	0.5	0.5	1

3.3. UV-Vis Spectroscopy

This characterization study investigates the optical properties of $LaFeO_3$ material doped with bismuth (Bi). Fig. 3 shows the reflectance results of $La_{0.5}Bi_{0.5}FeO_3$ nanoparticles. From the figure, it can be observed that there is an optical band gap of 2.1 eV. The DRS spectrum is similar to that of Fe_2O_3, indicating DRS responses due to Fe-O bonding. Electron transitions occur from the O 2p orbital in the valence band to the Fe 3d orbital in the conduction band [15].

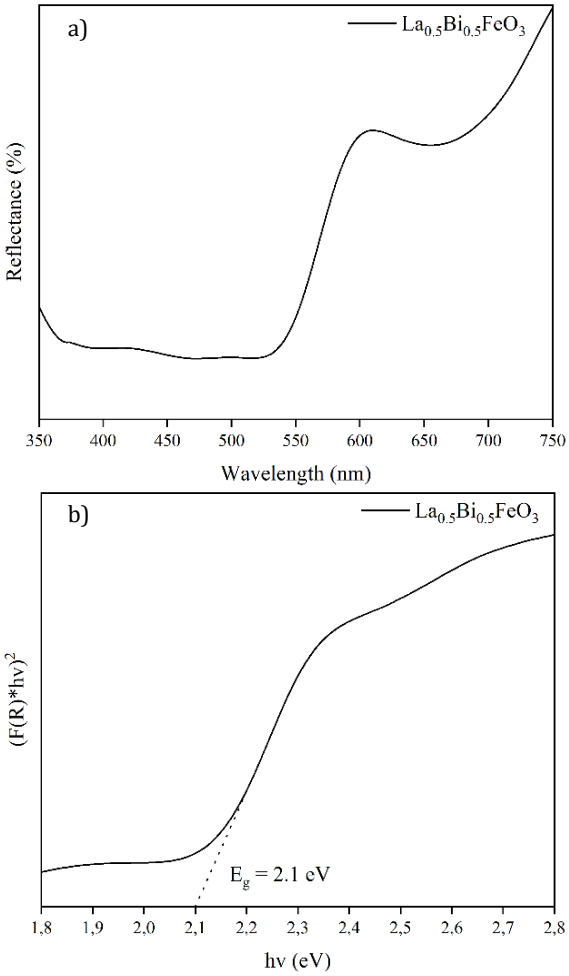


Fig. 3: The results of the $La_{0.5}Bi_{0.5}FeO_3$ (a) reflectance and (b) band gap characterization

3.4. Surface-Enhanced Raman Spectroscopy

Paraquat is an herbicide that belongs to the bipyridilium compound family (also referred to as bipyridyl), with the full chemical name 1,1′-dimethyl-4,4′-bipyridilium dichloride [CAS: 1910-42-5] [16]. This compound has the chemical composition $C_{12}H_{14}N_2$ and is one of the most widely used herbicides in agricultural lands [17]. This compound is composed of carbon (C), hydrogen (H), and nitrogen (N) atoms, as shown in Fig. 4 [18]. It is primarily composed of C-N, C=N, C-C, C=C, and C-H [19-21].

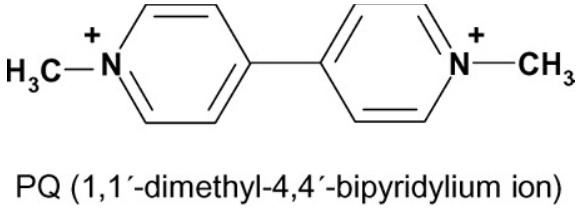


Fig. 4: Chemical structure of paraquat [22]

The SERS spectrum of paraquat at 6 ppm on different substrates is shown in Fig. 5. Pure SiO_2 substrate fails to provide substantial Raman enhancement for paraquat, as evident from the low signal intensity. The SiO_2-$La_{0.5}Bi_{0.5}FeO_3$ substrate without paraquat displays a Raman spectrum typical of $La_{0.5}Bi_{0.5}FeO_3$, featuring Fe O_6 phonon modes (500-750 cm^{-1}) and second-order scattering (above 1000 cm^{-1}) [9]. The blue spectrum displays significant signal enhancement which is a paraquat on the SiO_2-$La_{0.5}Bi_{0.5}FeO_3$ substrate. The green spectrum shows specific SERS signals for paraquat with peaks at 660, 842, 1192, 1285, 1538, and 1654 cm^{-1}. The signal which is purely from paraquat is obtained by subtracting the signal of the paraquat on SiO_2-$La_{0.5}Bi_{0.5}FeO_3$ substrate from that of SiO_2-$La_{0.5}Bi_{0.5}FeO_3$. This spectrum displays intense Raman bands at 660 cm^{-1} (ring deformation), 842 cm^{-1} (C-N stretching), 1192 cm^{-1} (C=C bending), 1285 cm^{-1} (C-C structural distortion), 1538 cm^{-1} (CH_2 bending + C-C stretching), and 1654 cm^{-1} (C=N stretching), as shown in Table 3 [1].

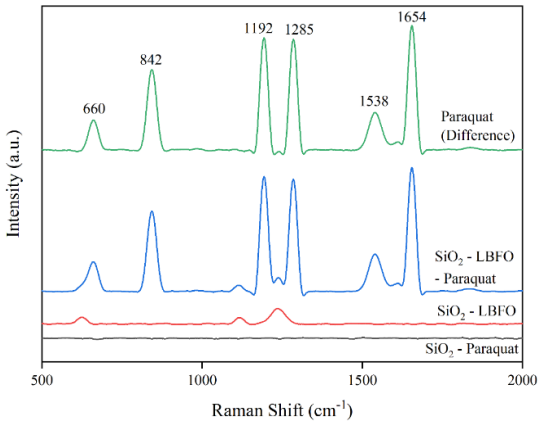


Fig. 5: Raman spectra of 6 ppm paraquat with different substrates

Table 3: Major band assignments of paraquat

Raman shift (cm^{-1})	Vibrational description
660	Ring deformation
842	ν(C-N)
1192	δ(C=C)
1285	C-C structural distortion
1538	δ(CH_2) + ν(C-C)
1654	ν(C=N)

ν-stretching; δ-bending

The precise mechanism underlying the enhancement of paraquat's SERS signals by LBFO is still under investigation. We hypothesize that the enhancement arises from photoinduced charge transfer, facilitated by LBFO's energy band gap of 2.1 eV. In addition, LBFO may serve as an intermediate medium that reduces the rapid attenuation of electromagnetic fields, thereby contributing to signal amplification [8]. A detailed account of our ongoing investigation into this enhancement mechanism will be presented in future work.

4. Conclusion

This study synthesized $La_{0.5}Bi_{0.5}FeO_3$ perovskite using the sol-gel method and deposited them onto silicon wafers as SERS substrates via the drop-casting technique. Characterization using XRD, XRF, and DRS confirmed the perovskite structure with high crystallinity, atomic composition consistent with stoichiometric calculations, and an optical bandgap of 2.1 eV. The SERS substrate demonstrated significant Raman signal enhancement for detecting trace amount of paraquat (6 ppm). These findings highlight the potential of $La_{0.5}Bi_{0.5}FeO_3$-based substrates for sensitive pesticide detection. In the future, advancements in LBFO-based substrates can focus on detecting other challenging molecules and incorporating them into portable devices for quick and efficient environmental monitoring.

Acknowledgment

This work was supported by research grants PPS-PTM 2025 from The Ministry of Higher Education, Science and Technology (Kemendiktisaintek) Republik Indonesia. The authors acknowledge the facilities and scientific and technical support from the Advanced Characterization Laboratory of National Research and Innovation Agency (ELSA BRIN). The authors would like to express their sincere gratitude for the support that made this research possible.

References

[1]. R. Botta, P. Eiamchai, M. Horprathum, S. Limwichean, C. Chananonnawathorn, V. Patthanasettakul, R. Maezono, A. Jomphoak, and N. Nuntawong, "3D structured laser engraves decorated with gold nanoparticle SERS chips for paraquat herbicide detection in environments" Sensors and Actuators B: Chemical, 304, (2020).

[2]. W. Chen, C. Li, Z. Yu, Y. Song, X. Zhang, D. Ni, D. Zhang, and P. Liang, "Optimum synthesis of cactus-inspired SERS substrate with high roughness for paraquat detection" Spectrochimica Acta Part A: Molecular and Biomolecular Spectroscopy, 268, (2022).

[3]. H. Pu, Y. Xie, Q. Wei, and D. W. Sun, "Anchoring Au on UiO-66 surface with thioglycolic acid for simultaneous SERS detection of paraquat and diquat residues in cabbage" Microchemical Journal, 190, (2023).

[4]. N. Lamei, M. Ezoddin, N. R. Kakavandi, K. Abdi, and M. Ghazi-khansari, "Ultrasound-Assisted Switchable Solvent in Determination of Quaternary Ammonium Herbicide Paraquat in Biological, Environmental Water, and Apple Juice Samples Using Chemical Reduction Process Coupled to GC-MS Detection" Chromatographia, 81(6), (2018).

[5]. C. Fuke, T. Arao, Y. Morinaga, H. Takaesu, K. Ameno, and T. Miyazaki, "Analysis of paraquat, diquat and two diquat metabolites in biological materials by high-performance liquid chromatography" Legal Medicine, 4(3), (2002).

[6]. A. Bauer, J. Luetjohann, S. Rohn, J. Kuballa, and E. Jantzen, "Development of an LC-MS/MS Method for Simultaneous Determination of the Quaternary Ammonium Herbicides Paraquat, Diquat, Chlormequat, and Mepiquat in Plant-Derived Commodities" Food Analytical Methods, 11(8), (2018).
[7]. H. Yu, Y. Peng, Y. Yang, and Z. Y. Li, "Plasmon-enhanced light-matter interactions and applications" npj Computational Materials, 5(1), (2019).
[8]. M. Awais, S. M. Z. A. Naqvi, Z. Wei, J. Wu, I. Arshad, V. Raghavan, S. U. Khan, and J. Hu, "Functionalized Single Crystal Perovskite Materials for SERS and Their Potential Detection Applications" Journal of Fluorescence, 35(5), 2467-2480 (2024).
[9]. D. Triyono, S. N. Fitria, and U. Hanifah, "Dielectric analysis and electrical conduction mechanism of La1-xBixFeO3 ceramics" RSC Advances, 10(31), (2020).
[10]. A. F. F. Alaih, D. Triyono, M. A. Dwiputra, and F. A. A. Nugroho, "Ultrafast and low-hysteresis humidity sensors based on mesoporous LaFe0.925Ti0.075O3 perovskite" Sensors and Actuators B: Chemical, 412, 135810, (2024).
[11]. V. Uvarov and I. Popov, "Metrological characterization of X-ray diffraction methods at different acquisition geometries for determination of crystallite size in nano-scale materials" Materials Characterization, 85, (2013).
[12]. T. Monecke, S. Köhler, R. Kleeberg, P. M. Herzig, and J. B. Gemmell, "Quantitative phase-analysis by the Rietveld method using X-ray powder-diffraction data: Application to the study of alteration halos associated with volcanic-rock-hosted massive sulfide deposits" The Canadian Mineralogist, 39(6), 1617–1633, (2001).
[13]. S. N. Fitria and D. Triyono, "The experimental investigation on the crystalline structure, lattice vibration, and optical energy of La1-xBixFeO3 nanoparticles" Journal of Physics: Conference Series, 1245, 012088, (2019).
[14]. K. Momma and F. Izumi, "VESTA: A three-dimensional visualization system for electronic and structural analysis" Journal of Applied Crystallography, 41(3), (2008).
[15]. M. Ismael and M. Wark, "Perovskite-type LaFeO3: Photoelectrochemical properties and photocatalytic degradation of organic pollutants under visible light irradiation" Catalysts, 9(4), (2019).
[16]. A. Calderbank, "The bipyridylium herbicides" Advances in Pest Control Research, 8, (1968).
[17]. L. S. Shabrina, Armen Ahmad, and Fadrian Fadrian, "Diagnosis and Management of Paraquat Intoxication" Bioscientia Medicina: Journal of Biomedicine and Translational Research, 7(8), (2023).
[18]. M. Lv, N. Hussain, D. W. Sun, and H. Pu, "Rapid detection of paraquat residues in fruit samples using mercaptoacetic acid functionalized Au@AgNR SERS substrate" Microchemical Journal, 189, (2023).
[19]. S. Asgari, L. Sun, J. Lin, Z. Weng, G. Wu, Y. Zhang, and M. Lin, "Nanofibrillar cellulose/Au@Ag nanoparticle nanocomposite as a SERS substrate for detection of paraquat and thiram in lettuce" Microchimica Acta, 187(7), (2020).
[20]. H. Fang, X. Zhang, S. J. Zhang, L. Liu, Y. M. Zhao, and H. J. Xu, "Ultrasensitive and quantitative detection of paraquat on fruits skins via surface-enhanced Raman spectroscopy" Sensors and Actuators B: Chemical, 213, (2015).
[21]. H. Luo, X. Wang, Y. Huang, K. Lai, B. A. Rasco, and Y. Fan, "Rapid and sensitive surface-enhanced Raman spectroscopy (SERS) method combined with gold nanoparticles for determination of paraquat in apple juice" Journal of the Science of Food and Agriculture, 98(10), (2018).
[22]. R. J. Dinis-Oliveira, J. A. Duarte, A. Sánchez-Navarro, F. Remião, M. L. Bastos, and F. Carvalho, "Paraquat poisonings: Mechanisms of lung toxicity, clinical features, and treatment" Critical Reviews in Toxicology, 38(1), (2008).
[23]. F. Z. Li, H. W. Zheng, M. S. Zhu, X. A. Zhang, G. L. Yuan, Z. S. Xie, X. H. Li, G. T. Yue, and W. F. Zhang, "Photovoltaic enhancement by Au surface-plasmon effect for la doped BiFeO3 films" Journal of Materials Chemistry C, 5(40), (2017).
[24]. A. Agrawal, S. H. Cho, O. Zandi, S. Ghosh, R. W. Johns, and D. J. Milliron, "Localized Surface Plasmon Resonance in Semiconductor Nanocrystals" Chemical Reviews, 118(6), (2018).
[25]. M. Wang, M. Ye, J. Iocozzia, C. Lin, and Z. Lin, "Plasmonic Photocatalysis: Plasmon-Mediated Solar Energy Conversion via Photocatalysis in Noble Metal/Semiconductor Composites" Advanced Science, 3(6), (2016).
[26]. M. T. Hossain, T. Jena, and P. K. Giri, "Recent Advances in the Growth Strategies, Multifunctional Properties, and Emerging Applications of Two-Dimensional Non-van der Waals Bismuth Oxychalcogenides and Prospective Heterostructures" Small Structures, 5(8), (2024).